Journal of Solid State Electrochemistry (2024) 28:1901–1908
https://doi.org/10.1007/s10008-023-05546-2

ORIGINAL PAPER

Effect of ceria on the properties of yttria-stabilized zirconia-based electrolytic membranes

D. A. Agarkov[1,6] · M. A. Borik[2] · G. M. Korableva[1] · A. V. Kulebyakin[2] · B. E. Komarov[2] · I. E. Kuritsyna[1] · E. E. Lomonova[2] · F. O. Milovich[3,4] · V. A. Myzina[2] · V. A. Pankratov[5] · N. Y. Tabachkova[2,4] · D. M. Zakharov[4]

Received: 19 April 2023 / Revised: 18 May 2023 / Accepted: 19 May 2023 / Published online: 25 May 2023

Abstract

$(ZrO_2)_{1-x-y}(Y_2O_3)_x(CeO_2)_y$ ($x = 0.08–0.10$; $y = 0.0–0.01$) solid solution crystals were grown by skull melting technique. The effects of CeO_2 addition on the crystal structure and high-temperature conductivity of the crystals have been investigated. According to X-ray absorption near-edge structure spectroscopy, it was found that Ce cations in crystals are present mainly as Ce^{4+} ions. The study of the grown crystals by X-ray diffraction, Raman spectroscopy, and transmission electron microscopy showed that all the grown crystals were single-phase and had either a tetragonal t`` or cubic structure, the latter having crystals containing 10 mol% Y_2O_3 and doped with CeO_2. Doping of the crystals with CeO_2 was accompanied by a linear increase in the lattice parameter. This indicates the entry of CeO_2 into the crystal lattice with the formation of a solid solution. The study of the ionic conductivity of crystals by impedance spectroscopy in the temperature range 400–900 °C showed that the substitution of Zr^{4+} ions with Ce^{4+} ions manifests itself in different ways and can either increase or decrease the value of high-temperature conductivity depending on the content of stabilizing yttrium oxide. Possible reasons for this behavior are discussed.

Keywords Zirconia · SOFC · Single crystal · Structure · Conductivity

Introduction

Zirconia-based solid solution systems have long been a subject of comprehensive research due to the great variety of their potential practical applications. These materials are used in the manufacture of oxygen pumps [1], electrolytic gas sensors [2], and as construction materials for thermal barriers and protective coatings. Zirconia-based materials are well-known solid state electrolytes [3–5] and widely used as electrolytic membranes in solid oxide fuel cells [6, 7]. The high oxygen-ionic conductivity of zirconia based solid solutions is attributed to the heterovalent substitution of zirconium cations by lower-valence cations, this process being accompanied by the formation of oxygen vacancies that are required for charge compensation. The concentration and type of the stabilizing oxide determines the structure of zirconia-based solid solutions and their physicochemical properties, e.g., electrophysical, thermophysical, and mechanical ones.

A large number of recent studies have dealt with the search for materials exhibiting chemical inertia and elevated ionic conductivity at medium temperatures (600–800 °C) [8]. Decreasing the operation temperatures of solid oxide fuel cells while retaining their high electrical conductivity is a critical task the solution of which will allow one to cut down the cost, increase the service life, raise the stability and reliability of solid oxide fuel cell components, and broaden the choice of potentially cheaper materials.

✉ D. A. Agarkov
agarkov@issp.ac.ru

1 Osipyan Institute of Solid State Physics RAS, Academician Osipyan Str, 2, 142432 Chernogolovka, Moscow District, Russia

2 Prokhorov General Physics Institute of Russian Academy of Sciences, Vavilova Street, 38, 119991 Moscow, Russia

3 Department of Materials Science, Moscow Polytechnic University, Bolshaya Semyonovskaya Street, 38, 107023 Moscow, Russia

4 Department of Materials Science of Semiconductors and Dielectrics, National University of Science and Technology (MISIS), Leninskiy Prospect, 4, 119049 Moscow, Russia

5 Institute of Solid State Physics, University of Latvia, 8 Kengaraga Iela, Riga 1063, LV, Latvia

6 Moscow Institute of Physics and Technology, Institusky Lane, 9, 141700 Dolgoprudny, Moscow Region, Russia

One of conventional materials used for the production of solid state electrolytes for electrochemical devices is yttria-stabilized zirconia (YSZ) exhibiting a good combination of promising mechanical, chemical, and electrolytic properties [9]. Since recently, the interest of researchers has been focused on zirconia-based solid solutions stabilized with several oxides that allow varying the physicochemical parameters of the target materials over a wide range. It has been shown that the use of several stabilizing oxides, for example, combined doping of zirconia with scandia and rare-earth elements, can increase the electrical conductivity and stability of the transport properties of zirconia-based solid solutions [10–12].

Along with zirconia, great attention is paid to the study of ceria-based solid state electrolytes. Rare-earth element doped ceria exhibits high electrical conductivity, as well as good thermodynamic stability [13] and catalytic activity [14]. Of great interest are also ZrO_2–CeO_2 solid solution-based materials additionally doped with rare-earth element oxides [8, 15–17].

Theoretical study [18] showed that the anion migration energy depends on the size of the doping element cation, the host matrix structure, and the host material cation size, whereas the association energy depends on the doping cation size. The authors stressed the importance of taking into account the interaction between the defects, including the formation of agglomerates from doping cations and oxygen vacancies. This type of interaction can be quite strong, especially at low temperatures which can be of great importance for practical applications. Experimental data on zirconia-based solid solutions stabilized with various rare-earth element oxides confirmed the tendency of a decrease in the activation energy of oxygen-ionic conductivity as the ionic radius of the stabilizing oxide cation approaches the ionic radius of the host material cation [19]. It was reported [17] that when the CeO_2 concentration changes, the electrical conductivity of ZrO_2–CeO_2–Y_2O_3 solid solutions is controlled by two processes: (1) the formation of defect clusters which reduce the mobility of oxygen vacancies and (2) an increase in the bulk electrical conductivity due to an increase in the lattice parameter resulting in a broadening of channels for the free migration of oxygen vacancies. Solid oxide fuel cell components, e.g., electrodes and electrolytes, exhibit substantial deviations from the oxygen stoichiometric concentration depending on whether the working media is oxidizing or reducing, as well as on the operation temperature and power consumption of the device. These parameters not only affect the electrical properties and phase stability of the material but also generate significant mechanical stresses due to changes in the lattice parameters caused by structural defects [20–22].

Earlier study of $(ZrO_2)_{1-x-y}(Sc_2O_3)_x(CeO_2)y$ crystals showed that the introduction of even low concentrations of CeO_2 (0.5 – 1 mol.%) affects the structure and high-temperature electrical conductivity of ZrO_2–Sc_2O_3 solid solutions [23].

The aim of this work is to study the effect of ceria on the structure and electrical conductivity of ZrO_2–Y_2O_3 solid solutions.

Materials and methods

$(ZrO_2)_{1-x-y}(Y_2O_3)_x(CeO_2)y$ solid solution crystals ($x = 0.08$–0.10; $y = 0.0$–0.01) were grown by the directional melt crystallization technique in a cold crucible [24]. The melt was crystallized in a 100 mm diameter water-cooled copper crucible at a 10 mm/h cooling rate. The raw materials were zirconia, yttria, and ceria powders of at least 99.99% purity. For this growth method, a thin sintered material layer formed between the melt and the crucible walls which prevented possible contact between the melt and the crucible metal and hence reduced the risk of melt contamination with extrinsic impurities. Random crystallization occurred at the crucible bottom. The crystals grew as the crucible is moved toward the cold zone. The growing ingot consisted of discrete single crystals that could be easily mechanically separated.

In order to identify cerium charge state in the crystals, X-ray absorption experiments have been carried out on the BALDER beamline at 3.0 GeV storage ring of MAX IV Laboratory [25]. The XANES spectra were measured in fluorescence detection mode by a 7-element silicon drift detector. Continuous energy scanning was carried out at a rate ~ 5 s per XANES spectrum. For each sample, 25 repeats were examined for possible radiation damage and afterwards accumulated into a resulting spectrum. The reference signal of Ce^{3+} has been measured in the same way in the cerium doped $Gd_3(Ga,Al)_5O_{12}$ single crystal. The reference CeO_2 sample was measured in transmission mode in order to avoid self-absorption distortion in such a concentrated sample.

The phase composition of the crystals was studied using X-ray diffraction and Raman spectroscopy. For the phase composition study, wafers were cut from the middle section of the crystals perpendicular to the < 001 > direction. X-ray diffraction study was carried out on a Bruker D8 diffractometer in CuKα radiation. For the Raman study, the excitation source was a 532 nm laser. The structure of the crystals was studied using transmission electron microscopy (TEM) under a JEM-2100 microscope at a 200 kV acceleration voltage. TEM specimens were prepared by ion beam thinning on a PIPS II plant. The initial wafers for thinning were cut from the crystals perpendicular to the < 110 > direction and processed to disks 3 mm in diameter and ~ 100 μm in thickness. In the centers of the disks, cavities were mechanically produced that were Ar ion beam thinned at the final specimen preparation stage.

The electrical conductivity of the zirconia-based crystals was studied in the 400–900 °C range with a Solartron SI 1260 frequency analyzer in the 1 Hz–5 MHz region at a 24 mV AC current signal. The specimens were in the form of 7 × 7 mm crystal wafers with a thickness of 0.5 mm. Electrical contacts were produced at two opposite wafer sides by burning-in platinum paste at 950 °C for 1 h in air. The impedance spectra were processed with the ZView software (version 2.8). The specific electrical conductivity of the crystals was calculated from the data obtained by impedance spectra processing with allowance for the dimensions of the specimens.

Results and discussion

For a study of the effect of CeO_2 doping on the properties of the crystals, one can arbitrarily divide the crystals in three series, i.e., $(ZrO_2)_{0.92-y}(Y_2O_3)_{0.08}(CeO_2)_y$ (series 1), $(ZrO_2)_{0.91-y}(Y_2O_3)_{0.09}(CeO_2)_y$ (series 2), and $(ZrO_2)_{0.90-y}(Y_2O_3)_{0.10}(CeO_2)_y$ (series 3) ($y = 0$; 0.005; 0.01). Hereinafter, the formula $(ZrO_2)_{1-x-y}(Y_2O_3)_x(CeO_2)y$ will be replaced for a brief notation of the 100_yCe100_xYSZ form, i.e., the compositions of series 1 crystals will be denoted as 8YSZ, 0.5Ce8YSZ, and 1Ce8YSZ; the compositions of series 2 crystals will be denoted as 9YSZ, 0.5Ce9YSZ, and 1Ce9YSZ; and the compositions of series 3 crystals will be denoted as 10YSZ, 0.5Ce10YSZ, and 1Ce10YSZ.

The as-grown crystals had columnar conical shapes with typical dimensions of 50 mm in height and 20 mm in the greatest cross-section. The crystals were homogeneous and transparent and had an orange-red hue the intensity of which increased with the CeO_2 content in the chemical composition of the crystal. The orange-red hue of the crystals originates from a wide absorption band in the 400 nm region which is attributed to the 4f → 5d transition of the Ce^{3+} ions [26].

Figure 1 shows the Ce ion (L_{III}-edge XANES) XANES spectrum for the 1Ce10YSZ crystal. The Ce^{3+} ion spectrum for aluminum-gallium-gadolinium garnet crystal is shown by way of comparison [27].

As can be seen from the data presented in Fig. 1, the XANES spectrum consists of two clear absorption bands peaking at 5731 and 5737 eV, which correspond to the Ce^{4+} ions [28]. Furthermore, the absorption band is broadened in the 5728 eV region which corresponds to the Ce^{3+} ions (marked by an arrow in the figure), indicating the presence of Ce^{3+} ions in the crystals. Thus, the as-grown crystals contain Ce in the form of both Ce^{4+} and Ce^{3+} ions, with the Ce^{4+} ions being noticeably more. This result, along with available literary data [29–31], allows accepting hereinafter that ceria in the crystals is mainly present in the form of Ce^{4+} ions.

According to the X-ray diffraction data, all the as-grown crystals were single-phase and had a fluorite-type cubic

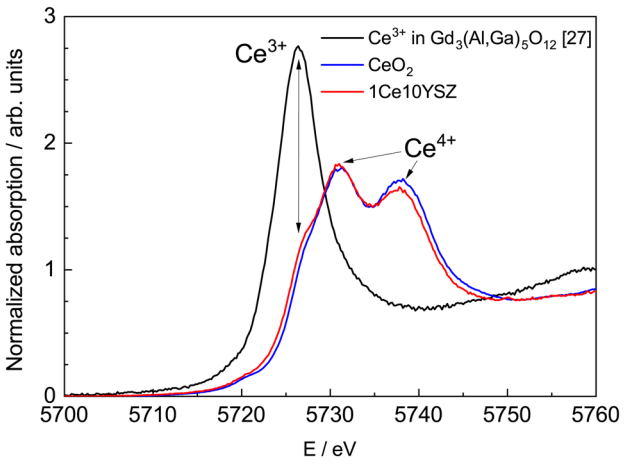

Fig. 1 Cerium LIII-edge XANES spectrum of 1Ce10YSZ single crystal (red line). The reference Ce^{3+} signal in cerium doped $Gd_3(Ga,Al)_5O_{12}$ is shown by black line [27], while the spectrum of the CeO_2 sample is given as a reference for $Ce.^{4+}$ centers (blue line)

structure. The diffraction pattern of the 1Ce10YSZ crystal is shown in Fig. 2. The pattern contains the second, fourth, and sixth order {001} plane reflections which are allowed for the Fm $\overline{3}$ m fluorite structure. This diffraction pattern is typical of all the as-grown crystals.

Figure 3 shows the lattice parameter of the material as a function of the Y_2O_3 content for different CeO_2 concentrations in the crystals. It can be seen from Fig. 3 that an increase in the Y_2O_3 concentration causes a linear increase in the lattice parameter of the material, the CeO_2 content being constant. CeO_2 addition also causes a monotonic increase in the lattice parameter. A similar change in the lattice parameters was also observed in [23, 32]. This lattice parameter vs. concentration relationship is quite expectable because doping with yttria and ceria leads to the incorporation into the cation sub-lattice of Ce^{4+} and Y^{3+} ions which are larger than the host matrix cations. Noteworthy, although the ionic radius of Y^{3+} (1.019 Å) is larger than that of Ce^{4+} (0.97 Å), ceria doping makes a greater contribution to the growth of the lattice parameter as compared with yttria doping. This can be accounted for by the fact that unlike isovalent substitution of Zr^{4+} by Ce^{4+}, heterovalent substitution of Zr^{4+} by Y^{3+} causes the formation of oxygen vacancies in the anionic sub-lattice which partially compensate the growth of the lattice parameter. Also, according to the XANES data, some of the Ce cations are in the Ce^{3+} state.

Raman data on the phase composition of the crystals are shown in Fig. 4. The spectra of the crystals containing 8 mol.% Y_2O_3 (Fig. 3a) contain bands that are typical of the tetragonal t`` phase [33]. This phase has a tetragonality degree of 1, and the oxygen ions in its lattice are shifted to the positions that are typical of a tetragonal structure [34,

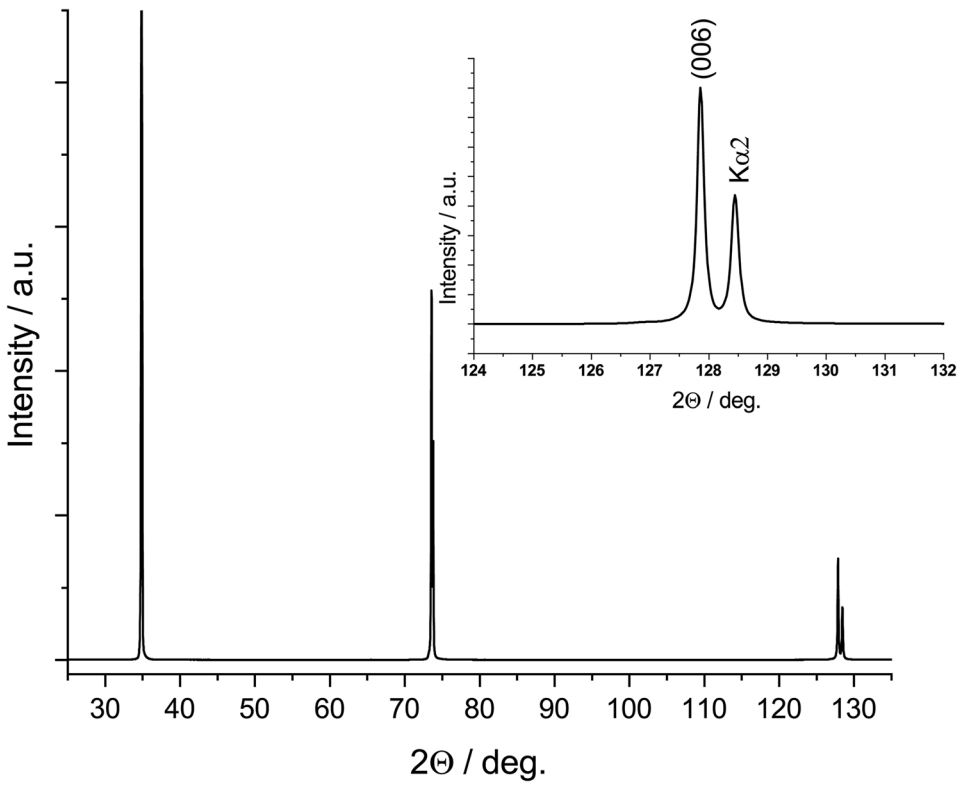

Fig. 2 Diffraction pattern of specimen cut from the 1Ce10YSZ crystal perpendicular to the < 001 > axis

35]. CeO_2 addition to the 8YSZ crystals reduces the intensity of the 244 cm^{-1} band, suggesting a decrease in the Zr-O bond length, and shifts the ~ 478 cm^{-1} band to greater wavelengths. Thus, the observed evolution of the Raman spectra for the $(ZrO_2)_{0.92-y}(Y_2O_3)_{0.08}(CeO_2)_y$ series of crystals with an increase in the CeO_2 content indicates that the structure of the t`` phase approaches that of a high-symmetry cubic phase. However, even at $y = 0.01$, these crystals retain a

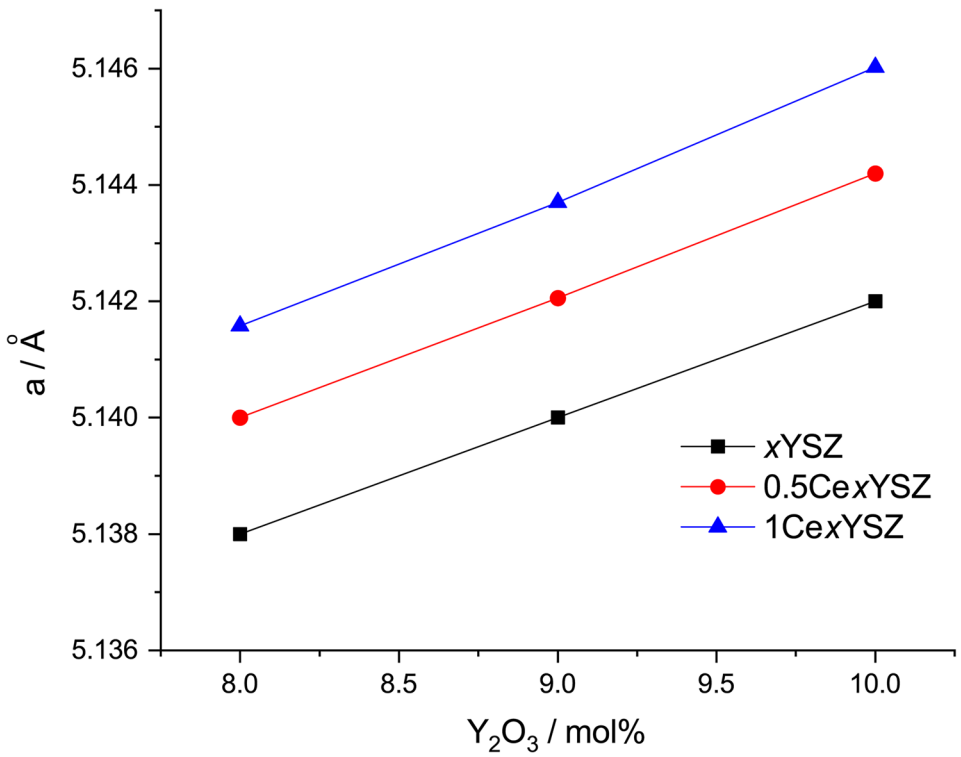

Fig. 3 Lattice parameters of the $(ZrO_2)_{1-x-y}(Y_2O_3)_x(CeO_2)_y$ crystals

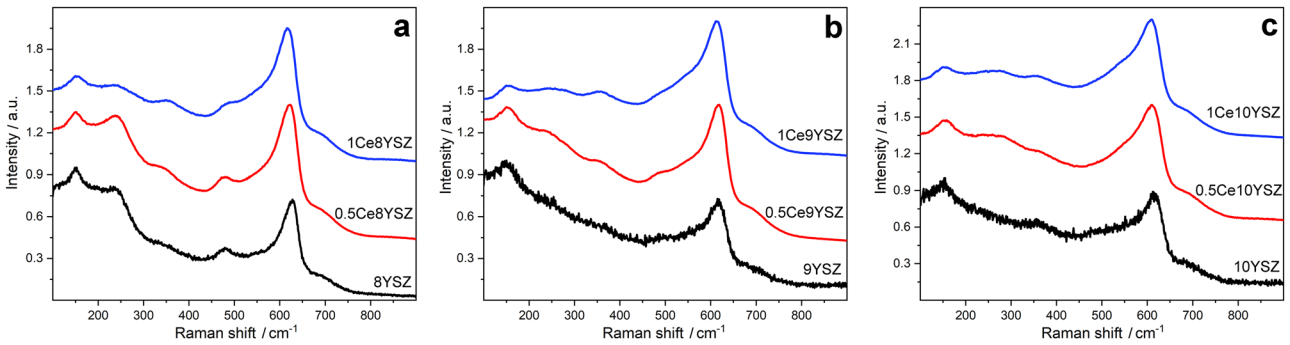

Fig. 4 Raman spectra of different crystal series: (**a**) $(ZrO_2)_{0.92-y}(Y_2O_3)_{0.08}(CeO_2)_y$, (**b**)—$(ZrO_2)_{0.91-y}(Y_2O_3)_{0.09}(CeO_2)_y$, and (**c**)—$(ZrO_2)_{0.90-y}(Y_2O_3)_{0.10}(CeO_2)_y$

tetragonal symmetry for the t`` phase. A similar tendency is observed for the $(ZrO_2)_{0.91-y}(Y_2O_3)_{0.09}(CeO_2)_y$ series of crystals. The spectra of all the crystals of this series also contain a weak but wide band at ~ 480 $cm^{-1}$ that is typical of the t`` phase. For the third series of solid solutions, i.e., $(ZrO_2)_{0.90-y}(Y_2O_3)_{0.10}(CeO_2)_y$, the band at ~ 480 cm^{-1} is only present in the spectra of the crystals not containing CeO_2 (10YSZ). Introduction of even 0.5 mol.% CeO_2 leads to a transformation of the spectrum corresponding to the pure cubic phase. Thus, the Raman data suggest that a high-symmetry fluorite-type phase forms in the 0.5Ce10YSZ and 1Ce10YSZ crystals only.

TEM studies of the structure and phase composition of the crystals confirmed the results obtained by Raman spectroscopy. The structures of the crystals pertaining to all the three series contained no visible defects such as inclusions, dislocations, and twins. The TEM images of the $(ZrO_2)_{1-x-y}(Y_2O_3)_x(CeO_2)_y$ were typical of low-defect single crystals. Bright-field images of the crystals mainly exhibited extinction contours originating from variations in the thickness of the test specimens. Electron diffraction patterns taken along the [110] zone axis of the first and second series crystals, i.e., $(ZrO_2)_{0.92-y}(Y_2O_3)_{0.08}(CeO_2)_y$ and $(ZrO_2)_{0.91-y}(Y_2O_3)_{0.09}(CeO_2)_y$, contained weak 001 and 110 type reflections. These reflections are not allowed for the Fm $\bar{3}$ m structure but are allowed for the P42/mnc one. The presence of the weak 001 and 110 type reflections may indicate a shift of the oxygen ions from their positions that are typical of a high-symmetry cubic phase, leading to a decrease in the symmetry of the crystals. For the crystals of the third series, i.e., $(ZrO_2)_{0.90-y}(Y_2O_3)_{0.10}(CeO_2)_y$, additional 001 and 110 type reflections were only observed in the electron diffraction patterns of the 10YSZ specimens. The electron diffraction patterns of the 0.5Ce10YSZ and 1Ce10YSZ crystals corresponded to the structure of a high-symmetry cubic phase. By way of example, Fig. 5 shows the electron diffraction patterns and structural images of the 1Ce8YSZ, 1Ce9YSZ, and 1Ce10YSZ crystals.

Thus, unlike the X-ray diffraction data, the Raman spectroscopy and transmission electron microscopy methods proved that the crystals of the first and the second series, i.e., $(ZrO_2)_{0.92-y}(Y_2O_3)_{0.08}(CeO_2)_y$ and $(ZrO_2)_{0.91-y}(Y_2O_3)_{0.09}(CeO_2)_y$, as well as the 10YSZ crystal, are not cubic but have the structure of the pseudo-cubic t`` phase in which the oxygen ions are slightly shifted along the C axis of the crystals. Of all the crystals studied herein, only the 0.5Ce10YSZ and 1Ce10YSZ have a fluorite-type cubic structure.

Data on the electrical conductivity of the crystals of all the three test series as a function of temperature are shown in Fig. 6 and in Table 1. It can be seen from Fig. 6 that the conductivity vs. temperature functions of the crystals of all the series are linear in Arrhenius coordinates and do not

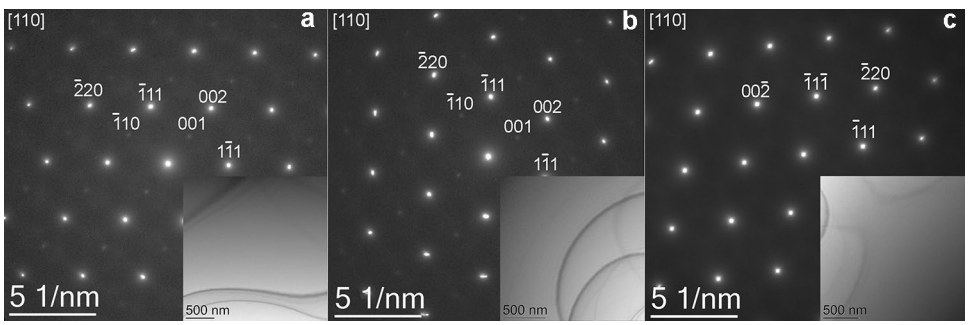

Fig. 5 Electron diffraction patterns of the (**a**) 1Ce8YSZ, (**b**) 1Ce9YSZ, and (**c**) 1Ce10YSZ crystals. Insets show bright-field TEM images of the crystals

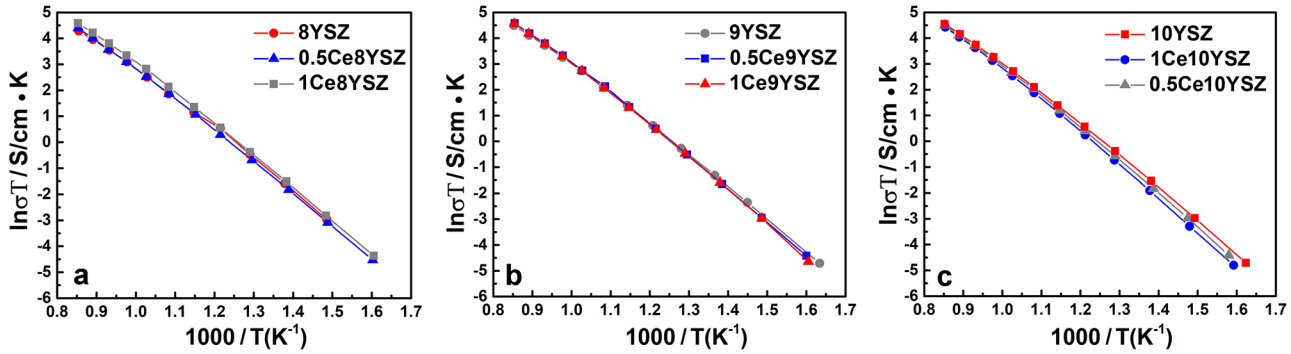

Fig. 6 Electrical conductivity as a function of temperature for crystals of different series: (**a**) $(ZrO_2)_{0.92-y}(Y_2O_3)_{0.08}(CeO_2)_y$, (**b**) $(ZrO_2)_{0.91-y}(Y_2O_3)_{0.09}(CeO_2)_y$, and (**c**) $(ZrO_2)_{0.90-y}(Y_2O_3)_{0.10}(CeO_2)_y$

intersect with one another. This indicates that the electrical conductivity of the crystals of each series changes monotonically in the entire experimental temperature range.

Figure 7 shows the 1173 K electrical conductivity of the crystals as a function of CeO_2 content for a constant yttria content.

It can be seen from Fig. 7 that CeO_2 doping of the crystals containing 8.0 and 9.0 mol.% Y_2O_3 (series 1 and 2) increased the high-temperature electrical conductivity of the crystals. On the contrary, CeO_2 doping of the crystals containing 10.0 mol.% Y_2O_3 (series 3) reduced their high-temperature electrical conductivity, i.e., the effect of Zr^{4+} ions substitution by Ce^{4+} ones varied depending on the content of stabilizing yttria. The growth of the electrical conductivity for the two former series of crystals can be attributed to the fact that the ionic radius of Ce^{4+} (0.97 Å) is greater than that of Zr^{4+} (0.84 Å) and closer to that of Y^{3+} (1.019 Å). According to numerous studies, the electrical conductivity of solid solutions based on zirconium dioxide depends on the position of oxygen vacancies relative to Zr^{4+} ions and cations of the stabilizing oxide [36–38]. The local structure is also affected by the difference in the sizes of the stabilizing oxide cation and the zirconium cation and the resulting lattice stresses.

Table 1 The values of the electrical conductivity of crystals at temperatures of 973 K, 1073 K, and 1123 K

Sample	Specific conductivity, S/cm		
	973K	1073 K	1123 K
8YSZ	0.0127	0.0324	0.0467
0.5Ce8YSZ	0.0128	0.0331	0.0488
1Ce8YSZ	0.0158	0.0400	0.0580
9YSZ	0.0158	0.0383	0.0550
0.5Ce9YSZ	0.0159	0.0412	0.0588
1Ce9YSZ	0.0172	0.0419	0.0603
10YSZ	0.0155	0.0391	0.0570
0.5Ce10YSZ	0.0146	0.0375	0.0541
1Ce10YSZ	0.0127	0.0350	0.0506

Thus, when yttrium ions are introduced into a solid solution based on zirconium dioxide, the resulting oxygen vacancy is predominantly located in the first coordination sphere of the zirconium cation [39]. The value of the potential barrier for the movement of an oxygen ion to the position of a vacancy upon interaction with cations that are surrounded by oxygen or an oxygen vacancy is given in [40]. The activation energy during oxygen migration through the edges of the Zr^{4+} – Zr^{4+}, Y^{3+} – Zr^{4+}, and Y^{3+} – Y^{3+} tetrahedra is 0.30, 0.85, 2.04 eV, respectively. This produces smaller lattice deformation, increases the lattice parameter, and provides for oxygen ion migration over oxygen vacancies [41]. Furthermore, for a smaller lattice deformation, the probability of oxygen vacancy localization in the vicinity of the trivalent Y^{3+} ions is lower while the probability of oxygen vacancy localization in the first coordination shell of Ce^{4+} is higher [42–44]. It is believed that this may reduce the probability of Coulomb interaction between the oxygen vacancies and the trivalent stabilizing oxide ions [45]. The above line of reasoning is probably also true for the third

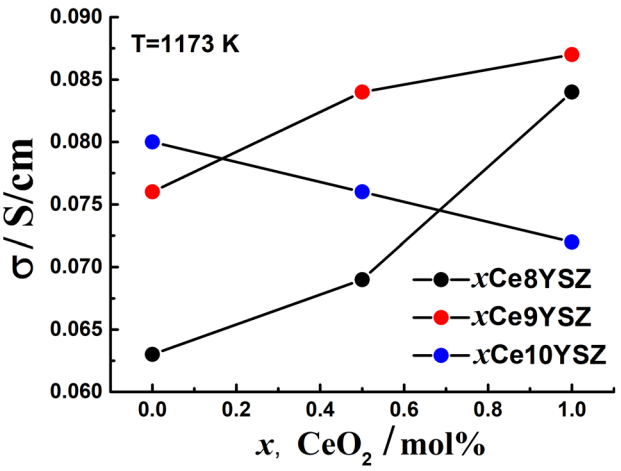

Fig. 7 1173 K electrical conductivity of the $(ZrO_2)_{1-x-y}(Y_2O_3)_x(CeO_2)_y$ crystals as a function of CeO_2 content

series of crystals, i.e., $(ZrO_2)_{0.90-y}(Y_2O_3)_{0.10}(CeO_2)_y$. However, in that case, the substitution of Zr^{4+} ions by Ce^{4+} ones entail a decrease in the high-temperature electrical conductivity of the material. There are other parameters that determine the electrical conductivity of a material, such as the crystal structure. Indeed, according to Raman spectroscopy and transmission electron microscopy data, only the 0.5Ce10YSZ and 1Ce10YSZ crystals have a fluorite-type cubic structure, whereas all the other crystals have a pseudo-cubic t`` phase structure. Furthermore, an increase in the CeO2 concentration entails an increase in the electrical conductivity activation energy. For example, the electrical conductivity activation energies of the 10YSZ, 0.5Ce10YSZ, and 1Ce10YSZ crystals as calculated for the 923–1173 K range were 0.90, 0.93, and 0.96 eV, respectively. In our opinion, the observed changes in the electrical conductivity can be caused by the structural transformation (t``→c) in the crystals. A decrease in the electrical conductivity with similar changes in the structure of ZrO_2–Y_2O_3 system crystals was observed earlier [46].

Conclusions

$(ZrO_2)_{1-x-y}(Y_2O_3)_x(CeO_2)_y$ solid solution crystals ($x = 0.08$–0.10; $y = 0.0$–0.01) were grown by the directional melt crystallization technique in a cold crucible. The as-grown crystals were transparent and had an orange-red hue caused by the presence of Ce^{3+} ions. An X-ray absorption near edge structure (XANES) study showed that the as-grown crystals contain ceria both in the form of Ce^{4+} and Ce^{3+} ions, with the Ce^{4+} ions being noticeably more. According to X-ray diffraction analysis, all the crystals were single-phase and had a fluorite-type cubic structure. A linear increase in the lattice parameter of the crystals was observed with an increase in the Y_2O_3 concentration and an increase in the CeO_2 concentration. This indicates that CeO_2 is incorporated into the lattice to form a solid solution. Raman spectroscopy and transmission electron microscopy studies of the crystalline structure of the solid solutions showed that only two crystals, i.e., 0.5Ce10YSZ and 1Ce10YSZ, had a fluorite-type cubic structure. The other crystals had the tetragonal t`` phase structure. We also showed that an increase in the $CeO_2$ content reduces the tetragonal distortion of the anion sub-lattice of the crystals and renders the structure of the t`` phase closer to that of a high-symmetry cubic phase. The study of the ionic conductivity of the crystals showed that the substitution of Zr^{4+} ions by Ce^{4+} ones exerts different effects on the material depending on the content of stabilizing ceria. For example, CeO_2 addition to the crystals containing 8.0 and 9.0 mol.% Y_2O_3 increases the high-temperature electrical conductivity of the crystals, whereas CeO_2 addition to the crystals containing 10.0 mol.% Y_2O_3 reduces their electrical conductivity. For the doping concentration range studied, the crystals doped with 1 mol.% CeO_2 and containing 8 and 9 mol.% Y_2O_3, i.e., the crystals having the t`` phase structure, had the highest electrical conductivity.

Acknowledgements The structure was investigated using the equipment of the center for collective use of scientific equipment "Material Science and Metallurgy," purchased with the financial support of the Ministry of Science and Higher Education of the Russian Federation (GK 075-15-2021-696). We acknowledge MAX IV Laboratory for time on Balder Beamline under Proposal 20200335. Research conducted at MAX IV, a Swedish national user facility, is supported by the Swedish Research council under contract 2018-07152, the Swedish Governmental Agency for Innovation Systems under contract 2018-04969, and Formas under contract 2019-02496. The Institute of Solid State Physics, University of Latvia as the Center of Excellence, has received funding from the European Union's Horizon 2020 Framework Program H2020-WIDESPREAD-01-2016-2017-TeamingPhase2 under grant agreement no. 739508, project CAMART2.

Funding This work was financially supported by the Moscow Polytechnic University within the framework of the grant named after Pyotr Kapitsa.

References

1. Pham AQ, Glass RS (1998) Oxygen pumping characteristics of yttria-stabilized-zirconia. Electrochim Acta 43:2699–2708
2. Maskell WC (2000) Progress in the development of zirconia gas sensors. Solid State Ion 134:43–50
3. Mahato N, Banerjee A, Gupta A, Omar S, Balani K (2015) Progress in material selection for solid oxide fuel cell technology: a review. Prog Mater Sci 72:141–337
4. Ramesh S, Ng CK, Tan CY, Wong WH, Ching CY, Muchtar A, Devaraj P (2016) Effects of sintering on the mechanical and ionic properties of ceria-doped scandia stabilized zirconia ceramic. Ceram Int 42:14469–14474
5. Ghazanfari A, Li W, Leu MC, Watts JL, Hilmas GE (2017) Additive manufacturing and mechanical characterization of high density fully stabilized zirconia. Ceram Int 43:6082–6088
6. Hibino T, Hashimoto A, Inoue T, Tokuno J, Yoshida S, Sano M (2000) A low-operating-temperature solid oxide fuel cell in hydrocarbon-air mixtures. Science 288(5473):2031–2033
7. Singhal SC (2002) Solid oxide fuel cells for stationary, mobile, and military applications. Solid State Ion 152–153:405–410
8. Zhigachev AO, Rodaev VV, Zhigacheva DV, Lyskov NV, Shchukina MA (2021) Doping of scandia-stabilized zirconia electrolytes for intermediate-temperature solid oxide fuel cell: a review. Ceram Int 47:32490–32504
9. Lv ZG, Yao P, Guo RS, Dai FY (2007) Study on zirconia solid electrolytes doped by complex additives. Mater Sci Eng A 458:355–360
10. Arachi Y, Asai T, Yamamoto O, Takeda Y, Imanishi N, Kawate K, Tamakoshi C (2001) Electrical conductivity of ZrO_2 Sc_2O_3 doped with HfO_2, CeO_2, and Ga_2O_3. J Electrochem Soc 148:A520
11. Xue Q, Huang X, Wang L, Zhang H, Zhang J (2018) Computational and experimental investigations of defect interaction and ionic conductivity in doped zirconia. Phys Rev Appl 10:014032
12. Agarkov DA, Borik MA, Bredikhin SI, Burmistrov IN, Eliseeva GM, Kolotygin VA, Kulebyakin AV, Kuritsyna IE, Lomonova EE, Milovich FO, Myzina VA, Ryabochkina PA, Tabachkova NYu, Volkova TV (2019) Structure and transport properties of zirconia

crystals co-doped by scandia, ceria and yttria. J Materiomics 5:273–279
13. Ju J-W, Huan D-M, Zhang Y-X, Xia C-R, Cui G-L (2018) Ionic conductivity of infiltrated Ln (Ln = Gd, Sm, Y)-doped ceria. Rare Met 37:734–742
14. Trovarelli A (2006) Catalytic properties of ceria and CeO2-containing materials. Catal Rev Sci Eng 38:439–520
15. Abbas HA, Argirusis C, Kilo M, Wiemhofer H-D, Hammad FF, Hanafi ZM (2011) Preparation and conductivity of ternary scandia-stabilised zirconia. Solid State Ion 184:6–9
16. Lee J-H, Yoon SM, Kim B-K, Kim J, Lee H-W, Song H-S (2001) Electrical conductivity and defect structure of yttria-doped ceria-stabilized zirconia. Solid State Ion 144:175–184
17. Yang F, Zhao X, Xiao P (2011) Bulk conduction and relaxation in [(ZrO2)1–x(CeO2)x]092(Y2O3)008 (0 ≤ x ≤ 1) solid solutions at intermediate temperatures. J Power Sources 196:4943–4949
18. Kilner JA, Brook RJ (1982) A study of oxygen ion conductivity in doped non-stoichiometric oxides. Solid State Ion 6(3):237–252
19. Arachi Y, Sakai H, Yamamoto O, Takeda Y, Imanishai N (1999) Electrical conductivity of the ZrO2 –Ln2O3 (Ln-lanthanides) system. Solid State Ion 121(1–4):133–139
20. Parkes MA, Refson K, d'Avezac M, Offer GJ, Brandon NP, Harrison NM (2015) Chemical descriptors of yttria stabilised zirconia at low defect concentration: an ab initio study. J Phys Chem A 119(24):6412–6420
21. Bishop SR, Tuller HL, Kuru Y, Yildiz B (2011) Chemical expansion of nonstoichiometric Pr01Ce09O2 − δ: correlation with defect equilibrium model. J Eur Ceram Soc 31(13):2351–2356
22. Marrocchelli D, Bishop SR, Tuller HL, Yildiz B (2012) Understanding chemical expansion in non-stoichiometric oxides: ceria and zirconia case studies. Adv Funct Mater 22(9):1958–1965
23. Agarkov DA, Borik MA, Bublik VT, Bredikhin SI, Chislov AS, Kulebyakin AV, Kuritsyna IE, Lomonova EE, Milovich FO, Myzina VA, Osiko VV, Tabachkova NYu (2018) Structure and transport properties of melt grown Sc2O3 and CeO2 doped ZrO2 crystals. Solid State Ion 322:24–29
24. Osiko VV, Borik MA, Lomonova EE (1987) Crucible-free methods of growing oxide crystals from the melt. Ann Rev Mater Sci 17(1):101–122
25. Klementiev K, Norén K, Carlson S, SigfridssonClauss KGV, Persson I (2016) The BALDER beamline at the MAX IV laboratory. J Phys: Conf Ser 712:012023
26. Orera VM, Merino RI, Pefia F (1994) $Ce^{3+}\leftrightarrow Ce^{4+}$ conversion in ceria-doped zirconia single crystals induced by oxido-reduction treatments. Solid State Ion 72:224–231
27. Kozlova AP, Kasimova VM, Buzanov OA, Chernenko K, Klementiev K, Pankratov V (2020) Luminescence and vacuum ultraviolet excitation spectroscopy of cerium doped Gd3Ga3Al2O12 single crystalline scintillators under synchrotron radiation excitations. Results Phys 16:103002
28. Lawrence NJ, Brewer JR, Wang L, Wu T-S, Wells-Kingsbury J, Ihrig MM, Wang G, Soo Y-L, Mei W-N, Cheung CL (2011) Defect engineering in cubic cerium oxide nanostructures for catalytic oxidation. Nano Lett 11(7):2666–2671
29. Lee CH, Choi GM (2000) Electrical conductivity of CeO_2-doped YSZ. Solid State Ion 135(1–4):653–661
30. Grazioli C, Hu Z, Knupfer M, Graw G, Behr G, Golden MS, Fink J, Giefers H, Wortmann G, Attenkofer K (2001) Characteristic temperature dependence of the 4f occupancy in the Kondo system CeSi2. Phys Rev B 63:115107
31. Khanin V, Venevtsev I, Chernenko K, Pankratov V, Klementiev K, Swieten T, Bunningen AJ, Vrubel I, Shendrik R, Rond C, Rodnyi P, Meijerink A (2021) Exciton interaction with Ce3+ and Ce4+ ions in (LuGd)3(Ga, Al)5O12 ceramics. J Lumin 237:118150
32. Yang F, Zhao X, Xiao P (2011) Bulk conduction and relaxation in $[(ZrO_2)_{1-x}(CeO_2)_x]_{0.92}(Y_2O_3)_{0.08}(0 \le x \le 1)$ solid solutions at intermediate temperatures. J Power Sources 196(11):4943–4949
33. Hemberger Y, Wichtner N, Berthold C, Nickel KG (2016) Quantification of yttria in stabilized zirconia by Raman spectroscopy. Int J Appl Ceram Technol 13(1):116–124
34. Yashima M, Ohtake K, Kakihana M, Arashi H, Yoshimura M (1996) Determination of tetragonal-cubic phase boundary of Zr1 − XRXO2 − X2 (R = Nd, Sm, Y, Er and Yb) BY Raman scattering. J Phys Chem Solids 57(1):17–24
35. Lukich S, Carpenter C, Orlovskaya N (2010) Temperature and stress induced changes of the vibrational response of cubic and rhombohedral 10 mol%Sc2O3–1 mol%CeO2–ZrO2 ceramics. J Power Sources 195(8):2301–2309
36. Araki W, Koshikawa T, Yamaji A, Adachi T (2009) Degradation mechanism of scandia-stabilised zirconia electrolytes: discussion based on annealing effects on mechanical strength, ionic conductivity, and Raman spectrum. Solid State Ion 180(28–32):1484–1489
37. Ding H, Virkar AV, Liu F (2012) Defect configuration and phase stability of cubic versus tetragonal yttria-stabilized zirconia. Solid State Ion 215:16–23
38. Zacate MO, Minervini L, Bradfield DJ, Grimes RW, Sickafus KE (2000) Defect cluster formation in M_2O_3-doped cubic ZrO_2. Solid State Ion 128(1–4):243–254
39. Borik MA, Volkova TV, Kuritsyna IE, Lomonova EE, Myzina VA, Ryabochkina PA, Tabachkova NY (2019) Features of the local structure and transport properties of ZrO_2-Y_2O_3-Eu_2O_3 solid solutions. J Alloys Compd 770:320–326
40. Shimojo F, Okazaki H (1992) Molecular dynamics studies of yttria stabilized zirconia. II. Microscopic mechanism of oxygen diffusion. J Phys Soc Jpn 61(11):4106–4118
41. Tsoga A, Naoumidis A, Stöver D (2000) Total electrical conductivity and defect structure of ZrO2–CeO2–Y2O3–Gd2O3 solid solutions. Solid State Ion 135(1–4):403–409
42. Li P, Chen I-W, Penner-Hahn JE (1994) Effect of dopants on zirconia stabilization — an X-ray absorption study: I, trivalent dopants. J Am Ceram Soc 77(1):118–128
43. Li P, Chen I-W, Penner-Hahn JE (1994) Effect of dopants on zirconia stabilization — an X-ray absorption study: II, tetravalent dopants. J Am Ceram Soc 77(5):1281–1288
44. Li P, Chen I-W, Penner-Hahn JE (1994) Effect of dopants on zirconia stabilization — an X-ray absorption study: III, charge-compensating dopants. J Am Ceram Soc 77(5):1289–1295
45. Lee J-H, Yoon SM, Kim B-K, Kim J, Lee H-W, Song H-S (2001) Electrical conductivity and defect structure of yttria-doped ceria-stabilized zirconia. Solid State Ion 144(1–2):175–184
46. Borik MA, Bredikhin SI, Bublik VT, Kulebyakin AV, Kuritsyna IE, Lomonova EE, Milovich FO, Myzina VA, Osiko VV, Ryabochkina PA, Tabachkova NYu, Volkova TV (2017) The impact of structural changes in ZrO_2-Y_2O_3 solid solution crystals grown by directional crystallization of the melt on their transport characteristics. Mat Lett 205:186–189